Proceedings of the ASME 2017 12th International Manufacturing Science and Engineering Conference
MSEC2017
June 4-8, 2017, Los Angeles, CA, USA

MSEC2017-2779

ACTIVE MIXING NOZZLE FOR MULTI-MATERIAL AND MULTI-SCALE 3D PRINTING

Hongbo Lan
Qindao Engineering Research Center for 3D Printing, Qingdao Technological University
Qingdao, Shandong, China

ABSTRACT

Multi-scale and multi-material 3D printing is new frontier in additive manufacturing. It has shown great potential to implement the simultaneous and full control for fabricated object including external geometry, internal architecture, functional surface, material composition and ratio as well as gradient distribution, feature size ranging from nano, micro, to marco-scale, embedded components and electro-circuit, etc. Furthermore, it has the ability to construct the heterogeneous and hierarchical structured object with tailored properties and multiple functionalities which cannot be achieved through the existing technologies. That paves the way and may result in great breakthrough in various applications, e.g., functional tissue and organ, functionally graded material/structure, wearable devices, soft robot, functionally embedded electronics, metamaterial, multi-functionality product, etc. However, very few of the established additive manufacturing processes have now the capability to implement the multi-material and multi-scale 3D printing. This paper presented a single nozzle-based multi-scale and multi-material 3D printing process by integrating the electrohydrodynamic jet (E-jet) printing and the active mixing multimaterial nozzle. The proposed AM technology has the capability to create multifunctional heterogeneously structured objects with control of the macro-scale external geometry and micro-scale internal structures as well as functional surface features, particularly, the potential to dynamically mix, grade and vary the ratios of different materials. An active mixing nozzle, as a core functional component of the 3D printer, is systematically investigated by combining with the theoretical analysis, numerical simulation and experimental verification. The study aims at exploring a feasible solution to implement the multi-scale and multi-material 3D printing at low cost.

INTRODUCTION

There is increasing demands for the ability to construct multifunctional heterogeneously structured objects with control of the macro-scale external geometry and micro-scale internal structures as well as functional surface features [1-10]. For example, researchers have begun to design biologically inspired robots (e.g., soft robotics) with soft or partially soft bodies, integrated sensors, electronics and functions and complex shapes [6.8], which have the potential to be more robust and adaptable, and safer for human interaction, than traditional rigid robots. To build a functional "wearable" device including its electronic components, a 3D printer would need to seamlessly transition from the flexible material that moves with the wearer's joints to the rigid material that holds the electronic components. It would also need to embed electrical circuitry with multiple inks of varying conductivity and resistivity, precisely switching between them. However, key challenges in the design and manufacture of such soft robots and wearable devices involve the complex multi-material and multi-scale fabrication processes, as well as the interfacing of soft and rigid components. It is critical difficult even impossible to construct such heterogeneous hierarchically structured objects by existing manufacturing technologies except adopting the emerging multi-material and multi-scale AM technologies.

The emerging multi-material and multi-scale 3D printing technique has shown great potential to implement the simultaneous and full control for fabricated object including external geometry, internal architecture, functional surface, material composition and ratio as well as gradient distribution, feature size ranging from nano, micro, to marco-scale, embedded components and electro-circuit, etc. It is able to construct the heterogeneous and hierarchical structured object with tailored properties and multiple functionalities which cannot be achieved through the existing technologies. Such technology has been considered as a revolutionary technology and next-generation manufacturing tool which can really fulfill the "creating material" and "creating life", especially subvert traditional product design and manufacturing scheme.

As additive manufacturing technology is quickly evolving from producing primarily single-material, homogenous objects to producing heterogeneous and hierarchical structured objects

Copyright © 2017 ASME

Downloaded From: http://proceedings.asmedigitalcollection.asme.org/pdfaccess.ashx?url=/data/conferences/asmep/93277/ on 07/28/2017 Terms of Use: http://www.asme.org/abo

with multi-functionality and tailored property, there is also a growing need for the multi-material and multi-scale 3D printing[11-16]. However, very few of the established additive manufacturing processes have the capability to implement the multi-material and multi-scale 3D printing. We proposed a novel multi-material and multi-scale 3D printing process which combined the electrohydrodynamic jet (E-jet) printing and the active mixing multimaterial nozzle technologies. Figure 1 demonstrated the basic principle of the multi-material and multi-scale 3D printing [17]. That offers a promising solution to implement the multi-scale and multi-material 3D printing at low cost. An active mixing nozzle is considered as one of the core functional components of the multi-material and multi-scale 3D printer. The focus of this paper is to perform a systematic investigation for the active mixing multi-material printhead by combining with the theoretical analysis, numerical simulation and experimental verification.

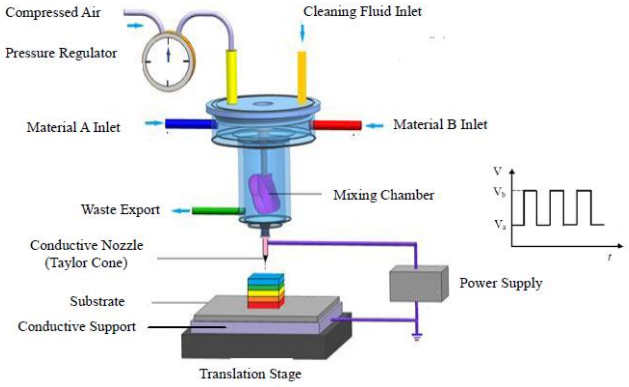

Figure 1. Schematic of multi-material and multi-scale 3D printing

MODELING OF ACTIVE MIXING NOZZLE

Figure 1 shows the structural diagram of the active mixing nozzle proposed. It consists of material A and B inlets, a compressed air inlet, cleaning fluid inlets, waste exports, a feed compartment, a mixing chamber, a conductive nozzle, and a mixing agitator. The mixing agitator includes a motor, screw impeller, and end cover.

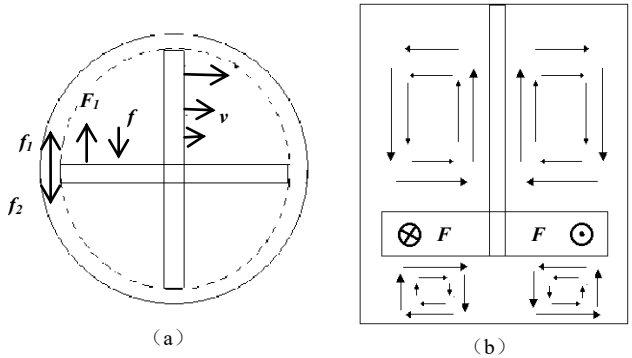

Figure 2. Force and structure of flow field in the mixing chamber (a) XY plane; (b) YZ plane

Assuming the impeller rotates clockwise at a low speed, the diagram of the stress on the fluid in an active mixing nozzle is shown in Figure 2(a). The force acting on the fluid, which is the volume force F, can be expressed as

$$\boldsymbol{F} = \boldsymbol{F_1} - \boldsymbol{f} + \boldsymbol{f_1} - \boldsymbol{f_2} \tag{1}$$

where F_1 is the mechanical force provided by the impeller; f is the resistance of the liquid on the impeller, f_1 represents the friction given by parts of the fluid in the impeller to the outer fluid of the impeller, and f_2 represents the resultant force of the inertial force and the friction force given by the wall to the fluid.

The rotating impeller can generates the centrifugal force and Coriolis force, which greatly influences viscous flow. Rotation causes turbulence flow and affects the stability of the boundary layer. Assuming the fluid in the active mixing nozzle is incompressible turbulent fluid, the physical equations that describe the mixing process consist of the flow control equation, standard k–ε equation, and diffusion equation.

Fluid Control Equation

Under the condition of constant temperature, for turbulent fluid with no changes in density and viscosity, the fluid continuity equation and momentum equation in vector form established under a rectangular coordinate system are, respectively,

$$\frac{\partial \rho}{\partial t} + \nabla \cdot (\rho \boldsymbol{u}) = 0 \tag{2}$$

$$\rho \frac{\partial \boldsymbol{u}}{\partial t} + \rho(\boldsymbol{u} \cdot \nabla)\boldsymbol{u} = \nabla \cdot \left[-p\boldsymbol{I} + (\mu + \mu_T)\left(\nabla \boldsymbol{u} + (\nabla \boldsymbol{u})^T\right) - \frac{2}{3}(\mu + \mu_T)(\nabla \cdot \boldsymbol{u})\boldsymbol{I} - \frac{2}{3}\rho k I \right] + \boldsymbol{F} \tag{3}$$

where $\boldsymbol{u}$ is the velocity vector of the fluid, ρ denotes the density of the fluid, μ *is* the dynamic viscosity of the fluid, $\boldsymbol{F}$ is the volume forces acting on the fluid, t is time, p is the pressure of the flow field, and k is the turbulence kinetic energy. The viscosity coefficient of the turbulence can be represented by the turbulence stress:

$$\mu_T = \rho C_\mu \frac{k^2}{\varepsilon} \tag{4}$$

where C_μ is a calculating constant.

In a turbulent motion with outer power impetus, the mechanical power provided by the motor is generally the only driving force. Compared to the driving forces, these forces including the friction force, shear force, and inertial force in the flow field are too small, which can even be neglected to simplify the calculation. As a result, the volume force acting on the fluid can be replaced by the resultant forces of the mechanical force $\boldsymbol{F_1}$ and the resistance force given by the fluid to the impeller $\boldsymbol{f}$, as in

$$\boldsymbol{F} = \boldsymbol{F_1} - \boldsymbol{f} \tag{5}$$

Copyright © 2017 ASME

Downloaded From: http://proceedings.asmedigitalcollection.asme.org/pdfaccess.ashx?url=/data/conferences/asmep/93277/ on 07/28/2017 Terms of Use: http://www.asme.org/abo

The resistance force given by the fluid to the impeller $\boldsymbol{f}$ is influenced by many factors, including the relative velocity of the impeller in the fluid, the contact area of the impeller and the fluid s, and the properties of the fluid (density, viscosity, etc.). Its computation formula is

$$f = \frac{1}{2} c\rho |\boldsymbol{v}|^2 s \tag{6}$$

where the resistance coefficient c is proportional to the viscosity; ρ is the density of the fluid.

Standard k–ε Equation

For the incompressible fluid without considering the source term, the transport equation for turbulent kinetic energy k and dissipated energy ε based on the k-ε turbulence model can be expressed as

$$\rho \frac{\partial k}{\partial t} + \rho(\boldsymbol{u} \cdot \nabla)k = \nabla \cdot \left[\left(\mu + \frac{\mu_T}{\sigma_k} \right) \nabla k \right] + p_k - \rho\varepsilon \tag{7}$$

$$\rho \frac{\partial k}{\partial t} + \rho(\boldsymbol{u} \cdot \nabla)\varepsilon = \nabla \cdot \left[\left(\mu + \frac{\mu_T}{\sigma_k} \right) \nabla \varepsilon \right] + C_{\varepsilon 1} \frac{\varepsilon}{k} p_k - C_{\varepsilon 2} \rho \frac{\varepsilon^2}{k} \tag{8}$$

where p_k is the generation item of turbulent kinetic energy k:

$$p_k = \mu_T \left[\nabla \boldsymbol{u} : \left(\nabla \boldsymbol{u} + (\nabla \boldsymbol{u})^T \right) - \frac{2}{3} (\nabla \cdot \boldsymbol{u})^2 \right] - \frac{2}{3} \rho k \nabla \cdot \boldsymbol{u} \tag{9}$$

ε is the dissipation rate of the turbulence, and the parameters of the turbulence model are

$$C_{\varepsilon 1} = 1.44, C_{\varepsilon 2} = 1.92, C_\mu = 0.09, \sigma_k = 1.3, \sigma_\varepsilon = 1$$

For the fluid in the active mixing nozzle, the Reynolds number can be expressed as

$$\mathrm{Re} = \frac{|\boldsymbol{u}| d}{\mu} \tag{10}$$

where $|\boldsymbol{u}|$ is the velocity of the fluid, d is the diameter of the active mixing nozzle, and μ is the dynamic viscosity of the fluid.

Diffusion Equation

Assuming that when two liquids mix, the properties (such as density and viscosity) of the liquids do not change, and the diffusion of more diluted material satisfies the law of conservation of mass

$$\nabla \cdot (-D_i \nabla c_i) + \boldsymbol{u} \cdot \nabla c_i = R_i \tag{11}$$

where c_i is the concentration of materials, D_i is the diffusion coefficient, $\boldsymbol{u}$ is the distribution of the velocity vectors in the velocity field, and R_i is a source term for the response to describe the change in the concentration of flow field.

Based on the above analysis, we can see that the flow of fluid in an active mixing nozzle with a mechanical impeller is a turbulent flow. These factors that may influence the mixing performance and efficiency involve the rotational speed of the impeller, the size of the impeller (diameter), and the viscosity of the fluid, among others. Furthermore, it is important to determine suitable process parameters for mixing material to achieve better blending performance and higher efficiency.

NUMERICAL SIMULATION

Calculation Methods

It was assumed that the fluid was incompressible Newtonian fluid with mutual seepage and dissolution, and that the flow was in a turbulence state. A tracer was introduced to facilitate observing the mixing effect of the fluid. The tracer was a tiny point with a clear color that would not affect the mixing of the fluid. The tracer was released through Gaussian pulse excitation.

The blending process of the tracer is a dynamic process that changes with time. The initial concentration of the tracer was set to 1, and other areas were set to 0. Mixing time was determined by observing the dispersion degree of the liquid in the tracer.

To achieve high-efficiency computation, we adopted the frozen rotor method to simulate the mixing of the fluid. Frozen rotor means the impeller and rotor are stationary. The fluid in the rotating field is presumed to be fixed in a rotating coordinate system. The effect of rotation is realized by introducing centrifugal force and Coriolis force.

Numerical Simulation Model

Figure 3 is a simplified sketch of the mixing chamber of the active mixing nozzle. The numerical simulation used a two-dimensional model. Figure 4 and Figure 5 show the structure of the mixing chamber and the location of the tracer respectively. The main parameters were as follows: the diameter of the mixing chamber was 40 mm, the interior diameter of the mixing chamber was 36 mm, the diameter of the impeller was 32 mm, and the rotating direction was clockwise.

A free triangular mesh was adopted, the size of the mesh cells used mesh refinement. Eventually, a complete mesh consisting of 14,252 domain units and 880 boundary units was generated.

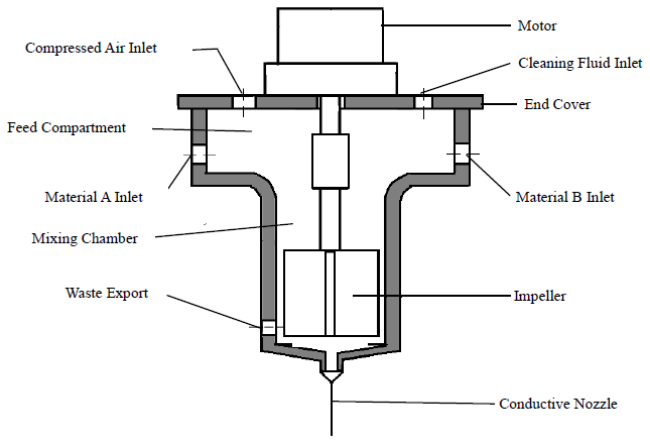

Figure 3. Schematic of the active mixing nozzle

Copyright © 2017 ASME

Downloaded From: http://proceedings.asmedigitalcollection.asme.org/pdfaccess.ashx?url=/data/conferences/asmep/93277/ on 07/28/2017 Terms of Use: http://www.asme.org/abo

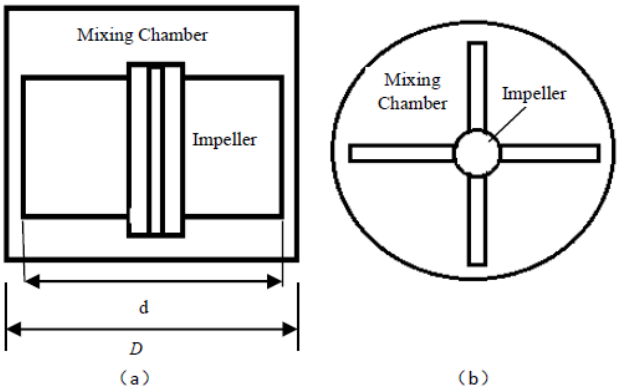

Figure 4. Simplified structure of the mixing chamber

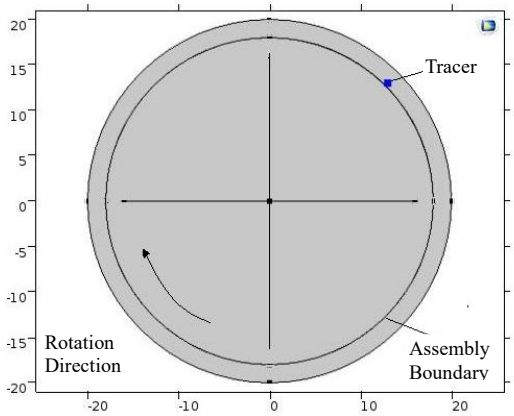

Figure 5. Diagram of the location of tracer

Numerical Simulation of Mixing Process

Assuming the fluid is not affected by friction, gravity, surface tension, and other factors, the temperature remains constant in the mixing process. The mixing medium was liquid resin with a density of 1,080 kg/m^3 and a dynamic viscosity of 20 cps. The rotational speed of the impeller was set to 20 r/min.

a) Analysis of the structure of the flow field

Figures 6(a) and 6(b) are diagrams of the velocity field and pressure field of the mixing chamber, respectively. Judging from the figure, if the distance between the center of rotation and the field is greater, the speed of the flow field will be higher, and the volume force on the fluid will be greater. If the speed of the flow field in the tip of the rotating impeller is at the highest level, it will face the largest volume force. Therefore, in the process of dynamic mixing, when adding other materials in the active mixing nozzle, the material should be added to the area where it can be swept by the tip of the active mixing nozzle's blade to the greatest extent to ensure that this material and the material in the nozzle are mixed fully and efficiently.

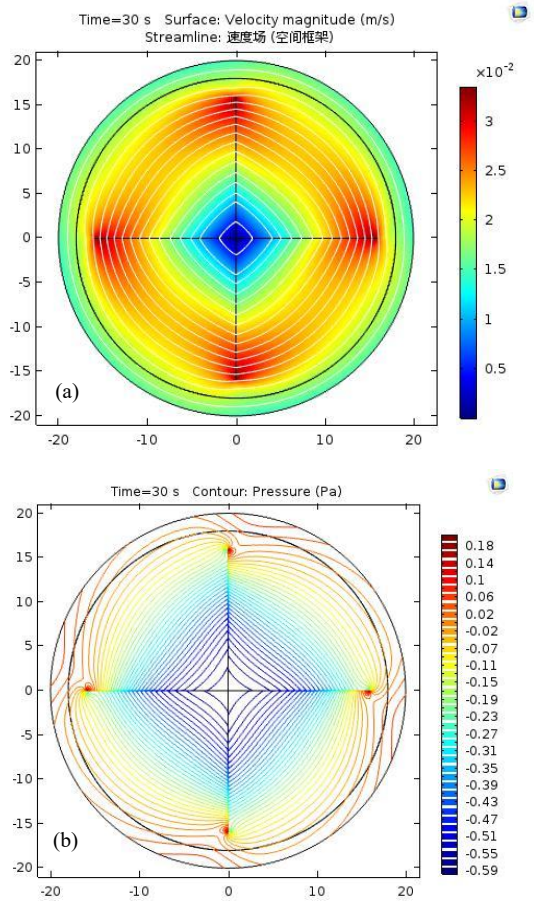

Figure 6. Velocity field and pressure field of the mixing chamber

(a) velocity field; (b) pressure field

b) Analysis of the mixing process

Figure 7 shows the tracer's mixing results in the mixing chamber at 0.9 s, 3.3 s, 7.2 s, 9.3 s, 12.9 s, and 18.3 s. Analyzing the figure reveals the following: When t = 0.9 s, the diffusion and mixing of the tracer are relatively slow. This is because the flow velocity and volume force of the tracer's releasing position are relatively small, which is not conducive to mixing the fluid. When t = 3.3 s, the distribution area of the tracer in the mixing chamber becomes larger. This is because the tracer comes into the high-speed area of the mixing chamber and mixes in all directions. As shown in Figure 7(d), it only takes a few seconds (t = 9.3 s) for the tracer to go throughout almost the entire mixing chamber. It takes a long time for the tracer to go from crossing the mixing chamber (t = 9.3 s) to fully mixing with the fluid (t = 18.3 s). This is because the slowest diffusion area is located near the center of the rotational impeller. Moreover, it takes a long time for the tracer and the fluid to fully mix. Therefore, when adding materials to the mixing chamber, the loading port should be located in the front area of the blade of the impeller.

Figure 8 shows the response curve of the tracer's concentration with the changes in mixing time. Based on the

Copyright © 2017 ASME

Downloaded From: http://proceedings.asmedigitalcollection.asme.org/pdfaccess.ashx?url=/data/conferences/asmep/93277/ on 07/28/2017 Terms of Use: http://www.asme.org/abo

figure, we can find that mixing efficiency is low at the beginning of the tracer's releasing phase. However, the mixing efficiency greatly increases later. When t > 7.2 s, the normalized response curve begins to flatten and mixing efficiency declines. When t = 12.9 s, the mixing degree of the tracer in the liquid is close to 95%. When t = 18.3 s, the tracer achieves complete mixing with the liquid. Thus, the active mixing nozzle can achieve highly efficient and even mixing among various materials in a relatively short period of time.

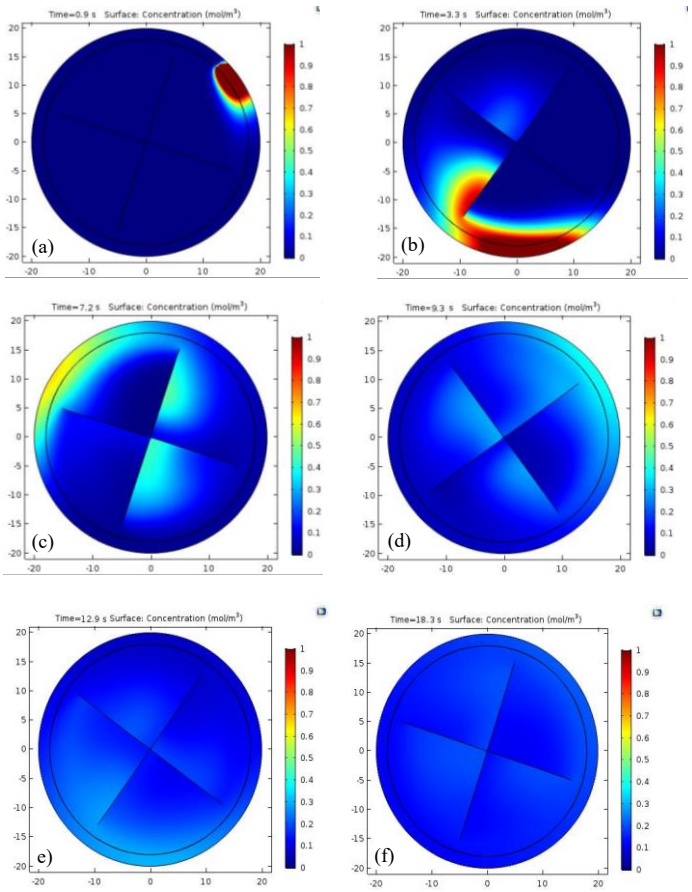

Figure 7. Mixing processs of tracer in the mixing chamber

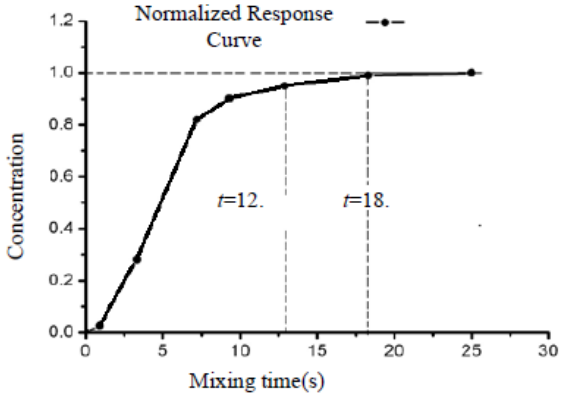

Figure 8. Response curve of tracer's concentration

Effects of the Mixing Process Parameters

a) Diameter of the impeller

The diameter of the impeller is a key factor influencing the performance of the active mixing nozzle. The chosen mixing medium was liquid resin with a density of 1,080 kg/m^3 and a viscosity of 20 cps. The rotational speed of the impeller was set to 20 r/min. Figure 9 shows the mixing effect of the fluid at t = 6 s with impeller diameters of 8 mm, 12 mm, 16 mm, 24 mm, 32 mm, and 34 mm. Figure 10 shows the curve of mixing time changes according to the diameter of the impeller.

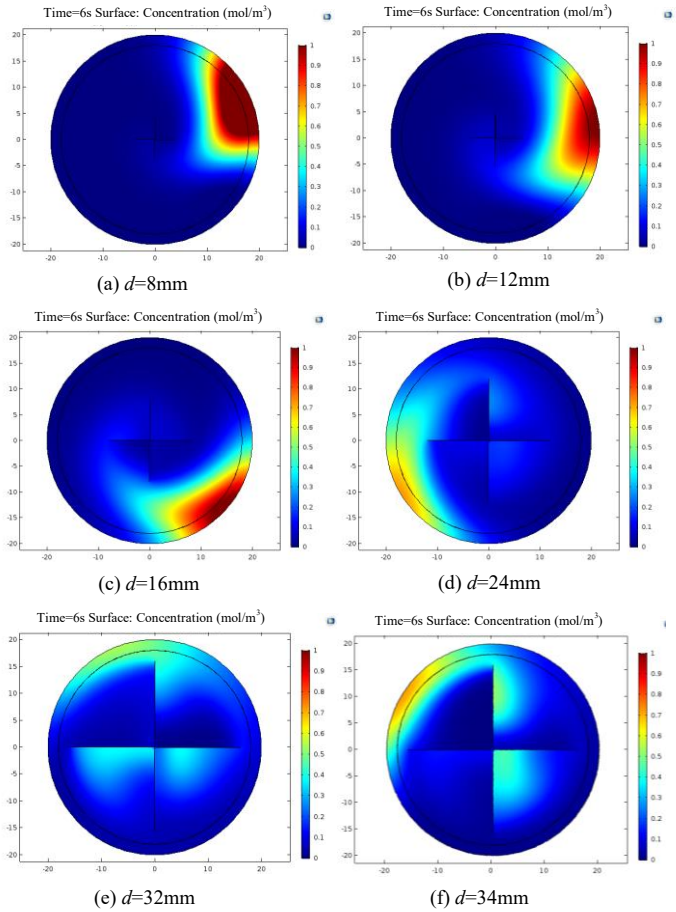

Figure 9. Mixing effect of the fluid at t = 6 s with different impeller diameters

The results show that when the diameter of the impeller d is less than 32 mm, the mixing efficiency of the fluid will increase with the increase in diameter. When the diameter is greater than 32 mm, mixing efficiency will decrease. The reasons for this are as follows. Under the condition of the same rotational speed, the size of the impeller's diameter determines the size of the volume force input by the impeller machine. If the diameter is smaller, the volume force input by the impeller machine will be smaller, causing the speed of the fluid in the mixing chamber to become slower and even decreasing the mixing effect. With an increase in the

Copyright © 2017 ASME

Downloaded From: http://proceedings.asmedigitalcollection.asme.org/pdfaccess.ashx?url=/data/conferences/asmep/93277/ on 07/28/2017 Terms of Use: http://www.asme.org/abo

impeller's diameter, the volume force input by the impeller machine will increase, and the fluid velocity will enlarge, improving mixing efficiency. However, when the diameter is greater than 32 mm, the space between the edge of the impeller and the interior wall of the mixing chamber will decrease, and the flow of fluid will be restricted. This is not conducive to the diffusion of the tracer in the fluid and can even cause uneven mixing with low efficiency. The mixing effect will also be affected. Based on the simulation results, mixing efficiency is higher when the diameter of the impeller is 28–32 mm for the given conditions.

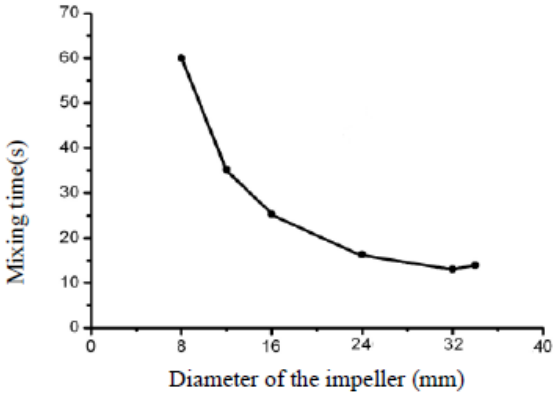

Figure 10. Mixing time changes with diameter of impeller

b) Rotational speed of the impeller

The rotational speed of the impeller is another important factor that influences the efficiency of an active mixing nozzle. The rotational speed of the impeller depends on the kinetic energy input of the motor and directly affects the diffusion effect of the fluid in the mixing nozzle. If impeller's rotational speed is optimal, it will not only reduce the motor's power consumption but will also have a good flow state and improve mixing efficiency.

The chosen mixing medium was liquid resin with a density of 1,080 kg/m^3 and a viscosity of 20 cps. The diameter of the impeller was set to 32 mm. Figure 11 shows the mixing effect of the fluid at t = 6 s with impeller rotational speeds of 5 r/min, 10 r/min, 20 r/min, 40 r/min, 50 r/min, and 60 r/min. Figure 12 shows the curve of mixing time changes according to the rotational speed of the impeller.

The results show that when the impeller's rotational speed is 5 r/min, the flow of the tracer in the fluid is very slow and mixing efficiency is low. With increased rotational speed, the flow speed of the tracer in the fluid increases and mixing efficiency is enhanced. The reasons for this are as follows. The rotational speed of the impeller determines the scale of the volume force in the mixing chamber. If the impeller's rotational speed is higher, the volume force in the mixing chamber will be greater, and the flow speed will higher. This is more conducive to diffusing the fluid and enhancing mixing efficiency. However, when the impeller's rotational speed exceeds 40 r/min, the mixing time will be further shortened, but the change will be slow. This is because many factors—not just the speed of the impeller—determine the mixing efficiency of the fluid. Therefore, considering power consumption and other factors, a faster speed is not necessarily better. The recommended optimal rotational speed is approximately 40 r/min.

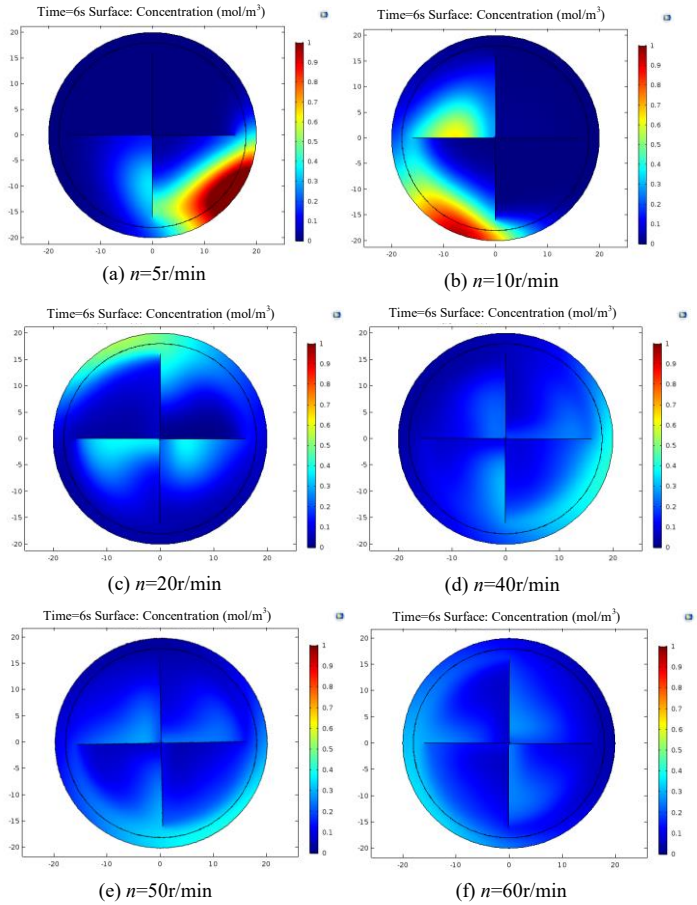

Figure 11. Mixing effect of the fluid with different rotational speeds of the impeller

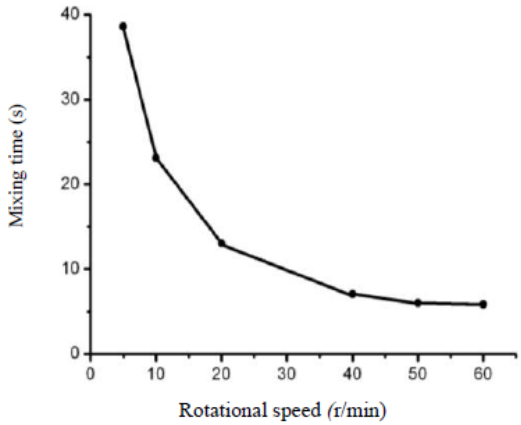

Figure 12. Mixing time changes with rotational speed of the impeller

Copyright © 2017 ASME

Downloaded From: http://proceedings.asmedigitalcollection.asme.org/pdfaccess.ashx?url=/data/conferences/asmep/93277/ on 07/28/2017 Terms of Use: http://www.asme.org/abo

c) Fluid viscosity

The mixing performance of an active mixing nozzle is not only associated with the process parameters of the nozzle itself but is also related to the physical properties of the mixing medium, especially the viscosity of the mixed fluid. This is because the viscosity of the mixed fluid directly determines the diffusion properties of the fluid.

The chosen mixing medium was liquid resin with a density of 1,080 kg/m^3 and a viscosity of 20 cps. The diameter of the impeller was 32 mm, and the rotational speed was 30 r/min. Figure 13 shows the mixing effect of the fluid at t = 6 s with fluid viscosities of 10 cps, 30 cps, 50 cps, 60 cps, 80 cps, and 100 cps. Figure 14 shows the curve of the mixing time changes according to viscosity.

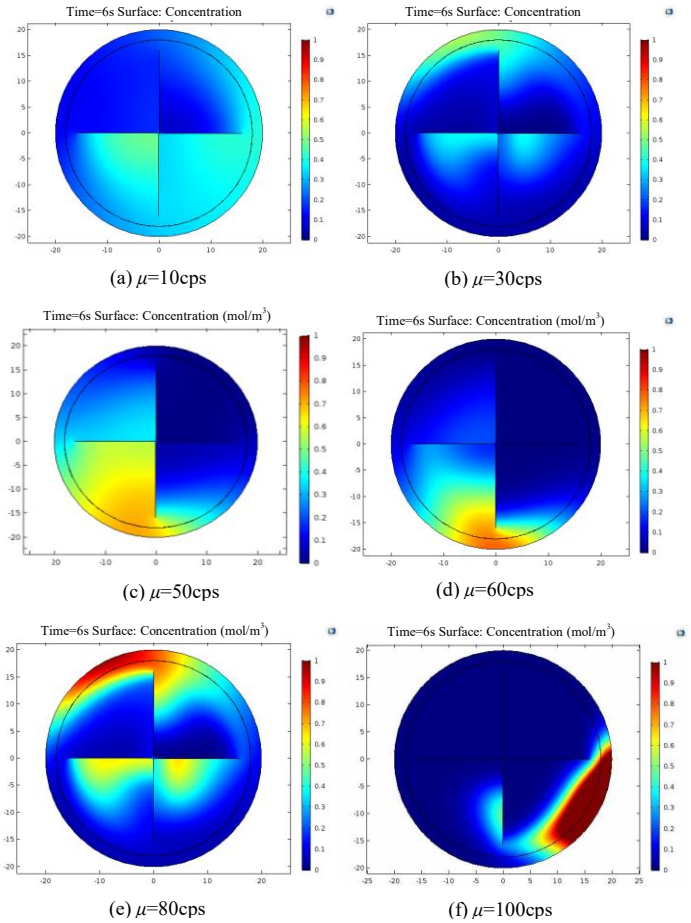

Figure 13. Mixing effect of the fluid with different fluid viscosities

The results show that when the viscosity is 10 cps, the mixing effect is better and mixing efficiency is higher. With increased viscosity, mixing efficiency will be reduced and mixing time will increase significantly. Comparing Figure 13 (c) and Figure 13 (d), we find that the mixing effect of the tracer in the fluid is better with a viscosity of 50 cps. When the viscosity is 80 cps, though the tracer disperses among the four blades, the distribution of the tracer is concentrated. The reasons are as follows. Viscosity determines the liquidity and diffusion of the fluid. The greater the viscosity of the fluid, the lower its liquidity, this is not conducive to spreading the fluid, and mixing time will increase. Therefore, suitable mixing times should be selected for fluids with different viscosities in order to achieve optimal mixing effect and mixing efficiency.

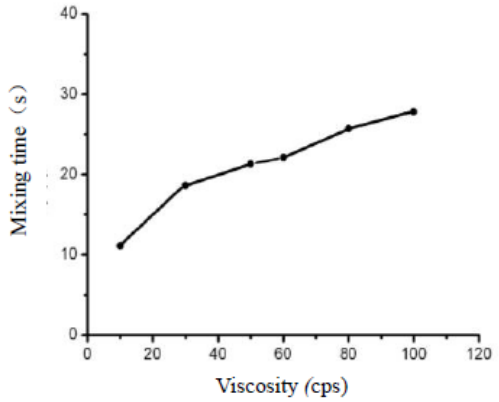

Figure 14. Mixing time changes with the viscosity of the fluid

EXPERIMENTS

Experimental equipment

Figure 15 shows the experimental equipment (setup) developed by our group. The diameter of the mixing chamber is 36 mm, and the impeller's diameter is 32 mm.

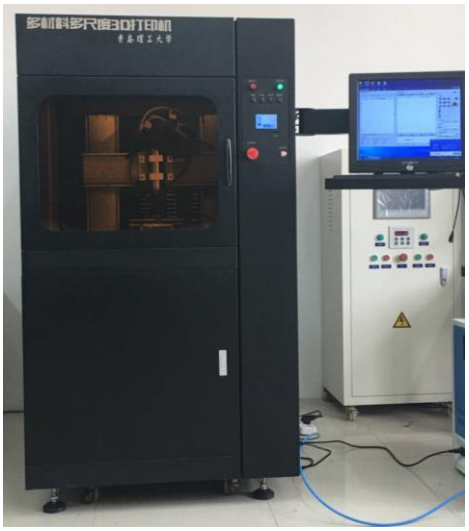

Figure 15. Experimental equipment

Gradient-colored models

The effect of the active mixing nozzle on mixing materials can be intuitively verified by examining printed gradient-colored models. The experimental material was liquid photosensitive resin; the specific performance of this material is shown in Table 1.

The used materials were white resin and blue resin.

Copyright © 2017 ASME

Downloaded From: http://proceedings.asmedigitalcollection.asme.org/pdfaccess.ashx?url=/data/conferences/asmep/93277/ on 07/28/2017 Terms of Use: http://www.asme.org/abo

They were provided to the active mixing nozzle in turn according to the volume ratios of the resin materials shown in Table 2. Based on the simulation results, the impeller's rotational speed was set to 30 r/min, and the stirring time was set as 22 s (mixing time was obtained when viscosity was 50 cps). The printed models are shown in Figure 16; 16 (a) is a cube model, and 16 (b) is a model of a cylinder. The experimental results demonstrate that the models had five layers in total. The color of each layer was relatively uniform. The entire model presented a gradient color. The experiment indicated that the active mixing nozzle can achieve uniform mixing between two kinds of resin materials in due time with high mixing efficiency.

Table 1. Property parameters for resin materials

Material	Color	Density (g/cm^3)	Viscosity (cps)	Yield Strength (MPa)	Elongation
Photosensitive resin	White	1.08	40	61.5	5%
Photosensitive resin	Blue	1.08	50	63	5%

Table 2. Material proportioning

Number of samples	Composition（w/%）	
	Blue resin	White resin
1	100	0
2	75	25
3	50	50
4	25	75
5	0	100

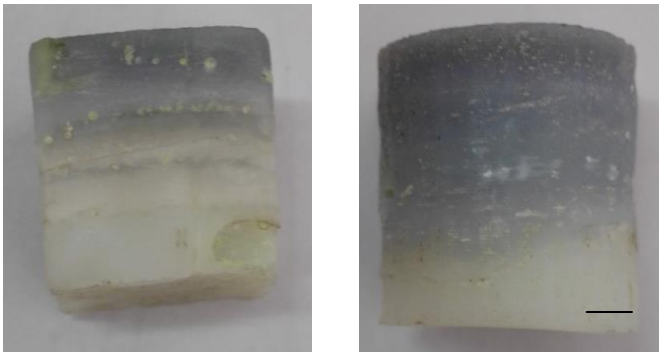

(a) *(b)*

Figure 16. Gradient-colored model printed (scale bar 2mm)

Variable stiffness models

The effect of an active mixing nozzle on mixing materials and its ability to realize integrated printing on multi-material were intuitively verified by measuring the hardness of variable stiffness models. This experiment adopted a flexible resin as the matrix and white resin as the additive (white resin can adjust the hardness of flexible resin). Table 3 shows the performance parameters of these two kinds of materials.

These two kinds of resin materials were added to the active mixing nozzle in turn following the volume proportions given in Table 4. Based on the simulation results, the rotational speed of the impeller was set to 30 r/min, and the stirring time was set as 25 s (mixing time was obtained when viscosity was 80 cps). Figure 17 shows the printed models of variable stiffness.

The hardness of the variable stiffness models in Table 17 were measured using a Shore durometer. The model with the same ratio was measured 5 times in different positions (the distance of each testing point was at least 6 mm). Table 5 shows the hardness values of the variable stiffness models. Table 5 shows that the hardness distribution of models printed by the same ratio of materials was uniform. This indicates that the active mixing nozzle can achieve the balanced mixing of two kinds of resin materials within 25 s with high mixing efficiency. This also verifies the reliability of the simulation results indicating that "the viscosity of the fluid will influence the mixing performance." With an increase in the proportion of white hard resin in the resin materials, the hardness of models printed by the active mixing nozzle also increased. A resin plate with gradient changes in hardness was ultimately obtained. This means that the active mixing nozzle can implement the integrated manufacturing of multiple different materials.

Table 3. Property parameters for resin materials

Material	Color	Density (g/cm^3)	Viscosity (cps)	Yield Strength (MPa)	Elongation
Photosensitive resin	White	1.08	40	61.5	5%
Flexible resin	Transparency	1.12	80	63	5%

Table 4. Material Proportioning

Number of samples	Composition（w/%）	
	Flexible resin	White resin
1	100	0
2	98	2
3	96	4
4	94	6
5	92	8

Table 5. Hardness of the models

Number of samples	Hardness of the models (HA)				
	A	B	C	D	E
1	64	62	64	62	65
2	68	68	67	69	66
3	73	73	74	72	74
4	76	77	76	75	76
5	80	82	82	86	80

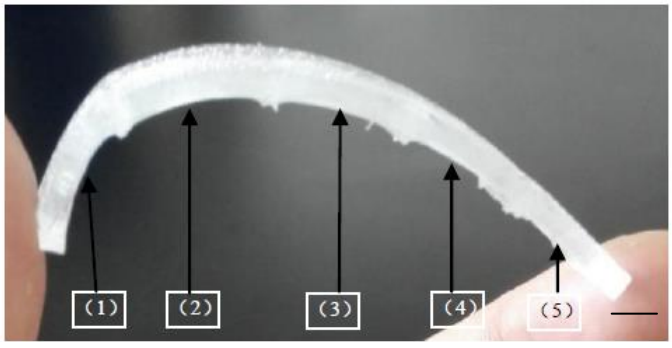

Figure 17. Variable stiffness model (scale bar5mm)

Micro-scale models

Figure 18 shows the printed modes with micro scale features. Different line width patterns have been printed using the same needle with a diameter of 60μm, as shown in Figure 19.

Copyright © 2017 ASME

Downloaded From: http://proceedings.asmedigitalcollection.asme.org/pdfaccess.ashx?url=/data/conferences/asmep/93277/ on 07/28/2017 Terms of Use: http://www.asme.org/abo

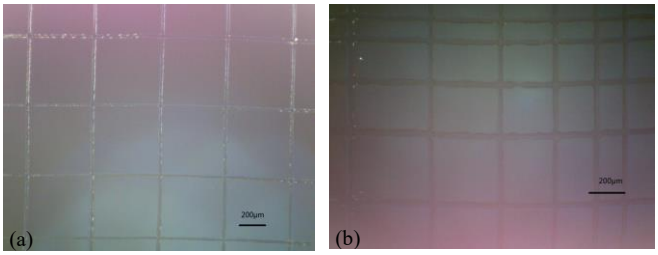

Figure 18. Micro scale models (a)uniform grid ; (b)non-uniform grid

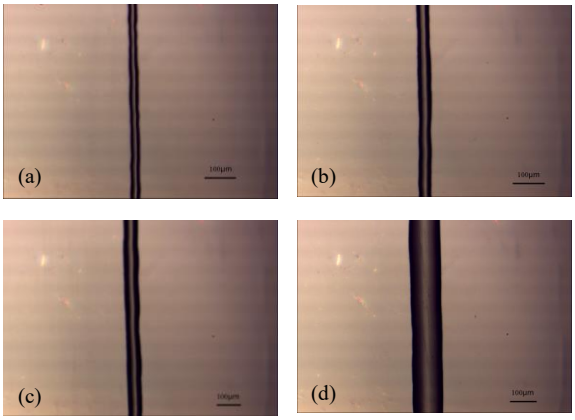

Figure 19. Different line width patterns printed using the same needle with a diameter of 60μm (a) 25μm;(b) 40μm;(c) 60μm;(d) 110μm

CONCLUSIONS

Multi-scale and multi-material 3D printing has the potential to accelerate innovation – engineers and researchers will have the power to create objects that have been previously impossible or very difficult to fabricate. Multi-material AM has become a powerful fabrication tool that adds on two extra dimensions in the available design space. Recent advances in additive manufacturing are enabling a shift from a geometry-centric to a material-centric design practice. In particular, the integrated design of "structure-material-performance-process" was introduced. Multi-material 3D printing has been considered as next generation AM technology. The ability to integrate disparate materials and properties within printed objects is the next frontier in 3D printing. This paper presented an active mixing nozzle for implementing a multi-scale and multi-material 3D printing process proposed. The active mixing nozzle has shown great potential to fulfill multi-material additive manufacturing with high efficiency and low cost. That made it possible to 3D print more complex and gradient architectures, thus allowing for better quality manufacturing of soft robotics, wearable devices, FG materials/structures, tissue organs, and other embedded electronics as well as structure electronics.

ACKNOWLEDGMENTS

This work was financially supported by National Science Foundation of China (No.51375250).

REFERENCES

[1] Derby B. Printing and prototyping of tissues and scaffolds. Science, 2012, 338(6): 6109.

[2]Lewis J A, Ahn B Y. Device fabrication: Three-dimensional printed electronics. Nature, 2015, 518: 42–43.

[3]Vaezi M, Chianrabutra S, Mellor B, et al. Multiple material additive manufacturing Part 1: a review. Virtual and Physical Prototyping. 2013, 8(1): 19-50.

[4] Kokkinis D, Schaffner M, Studart A R. Multimaterial magnetically assisted 3D printing of composite materials. Nature Communications. 2015, 6: 8643.

[5] Wegst U G K, Bai H, Saiz E, et al. Bioinspired structural materials. Nature Materials. 2015, 14: 23-36.

[6] Wehner M, Truby R L, Fitzgerald D J, et al. An integrated design and fabrication strategy for entirely soft, autonomous robots. Nature. 2016, 536: 451-455.

[7] Oxman N. Variable property rapid prototyping. Virtual and Physical Prototyping. 2011, 6(1): 3-31.

[8] Bartlett N W, Tolley M T, Overvelde J T B, et al. A 3D-printed, functionally graded soft robot powered by combustion. Science. 2015, 349(6224): 161-165.

[9] Park J U, Hardy M, Kang S J, et al. High-resolution electrohydrodynamic jet printing. Nature Materials, 2007, 6(10): 782-789.

[10] Rahman T, Renaud L, Heo D, et al. Aerosol based direct-write micro-additive fabrication method for sub-mm 3D metal-dielectric structures. J. Micromech. Microeng. 2015, 25: 107002.

[11] Chimate C and Koc B. Pressure assisted multi-syringe single nozzle deposition system for manufacturing of heterogeneous tissue scaffolds. Int J Adv Manuf Technol. 2014, 75:317–330.

[12] Hohmann J K, Renner M, Waller E H, et al. Three-Dimensional μ-printing: an enabling technology. Adv. Optical Mater. 2015, 3:1488–1507.

[13] Oropallo W and Piegl L A. Ten challenges in 3D printing. Engineering with Computers. 2016, 32(1): 135–148.

[14] Hardin J M, Ober T J, Valentine A D, et al. Microfluidic printheads for multimaterial 3D printing of viscoelastic inks. Adv. Mater. 2015, 27: 3279–3284.

[15] Hessel V, Löwe H, Schönfeld F, Micromixers—a review on passive and active mixing principles. Chem Eng Sci. 2005,60(8):2479–2501.

[16] Ober T J, Foresti D, Lewis J A. Active mixing of complex fluids at the microscale. PNAS. 2015, 112(40): 12293–12298.

[17] Lan H. Apparatus and method for multi-material and multi-scale 3D printing using single nozzle. PCT/CN2016/096337.

Copyright © 2017 ASME

Downloaded From: http://proceedings.asmedigitalcollection.asme.org/pdfaccess.ashx?url=/data/conferences/asmep/93277/ on 07/28/2017 Terms of Use: http://www.asme.org/abo